

Paleomagnetic Measurement of Nonbrittle Coseismic Deformation Across the San Andreas Fault at Pallett Creek

STEPHEN L. SALYARDS¹

Seismological Laboratory, California Institute of Technology, Pasadena

KERRY E. SIEH AND JOSEPH L. KIRSCHVINK

Division of Geological and Planetary Sciences, California Institute of Technology, Pasadena

Paleomagnetic data have been obtained to address a problem at the Pallett Creek paleoseismological site: the 9 mm/yr slip rate determined from three-dimensional mapping of late Holocene offsets across discrete faults is only a quarter of the expected value. We suspected that nonbrittle deformation adjacent to the faults might account for the 26 mm/yr discrepancy. In our search for the missing slip we collected and analyzed 264 paleomagnetic samples from a 53-m-wide transect across the fault zone. Half the samples came from a unit deposited immediately after a large earthquake of about A.D. 1480; these samples were affected by two large earthquakes that involved rupture at the site in 1812 and 1857. We collected the other half of the samples from a slightly older bed, one that was deposited before the earthquake of about A.D. 1480. Relative to "control" groups composed of 10 samples and collected 50 m from the fault, samples closer to the fault display clockwise rotations of 30° or less. If interpreted as block rotations, the data from the older unit imply that it has sustained a total of 14.0 ± 2.9 m of dextral warp during the past three major earthquakes and that the younger unit has experienced a total of 8.5 ± 1.0 m of warp during the most recent two. Combining these values with the amounts of dextral slip across the mapped fault planes yields dextral offsets of 5.5, 6.25, and 6.25 m for the events of A.D. 1480, 1812, and 1857 and a slip rate of 35.6 ± 6.7 mm/yr. This slip rate, averaged over the past three complete seismic cycles, is consistent with published rates from other sites. Offsets associated with the past three events are remarkably similar. These amounts, however, appear independent of the length of interseismic cycles. These observations suggest (1) that this part of the San Andreas fault has a characteristic strength and (2) that conventional concepts of strain accumulation and relief (for example, time- and slip-predictable models of earthquake occurrence) are unrealistic.

INTRODUCTION

Motion across a fault zone may result in two types of deformation. Brittle deformation is expressed as discrete offset across narrow fault planes and fractures. Nonbrittle deformation, or warp, is expressed as rotations within the fault zone, with the amount of rotation generally increasing toward the fault zone.

Because it is more difficult to recognize and quantify, nonbrittle deformation is only rarely evaluated in paleoseismic and neotectonic studies. This omission may result in an underestimation of both the offset magnitude associated with individual faulting events and the rate of fault slip. Such underestimates may significantly affect kinematic interpretations and evaluations of seismic hazard. For example, calculation of earthquake recurrence intervals by division of measured brittle slip by a geodetically determined slip rate may underestimate actual intervals. Also, variations in the slip rate of a fault, determined from studies at different locations along strike, may be misinterpreted as having regional tectonic significance, when, in fact, the variations are due to variable amounts of undetected nonbrittle deformation.

Measurement of nonbrittle deformation is usually difficult and often impossible. In pervasively deformed rocks, distor-

tion of fossils, pebbles, and other shapes with known original dimensions may enable estimation of nonbrittle deformation [Ramsay and Huber, 1983]. Anomalous bends in reference lines that cross faults at high angles may also be used to estimate nonbrittle deformation [Nelson and Jones, 1987], but this is hampered by the fact that the initial linearity of such features is commonly difficult to prove.

The most relevant study of deformed reference lines may well be a study of fence lines disrupted by the San Andreas fault during the 1906 San Francisco earthquake [Thatcher and Lisowski, 1987]. These fences show that 0-60% of the total right-lateral deformation across the fault zone occurred as nonbrittle warping.

In some cases, the nonbrittle deformation in a sediment or rock may be estimated from paleomagnetic data. A synchronously deposited body of rock or a stratum should acquire the magnetic field direction existing at the time of its deposition. Vertical axis rotation of the rock mass or stratum will result in changes in the declination of the remanent magnetization. Comparison between paleomagnetic directions and a reference direction appropriate for the undeformed rocks should enable quantitative analysis of the total rotation and deformation.

In this study, we apply paleomagnetic investigations to a significant problem of nonbrittle deformation in late Holocene sediments along the San Andreas fault.

PROBLEMS AT PALLETT CREEK

For several years the Pallett Creek paleoseismic site, 55 km northeast of Los Angeles, has presented a disturbing

¹Now at Geophysics Program, New Mexico State University, Las Cruces.

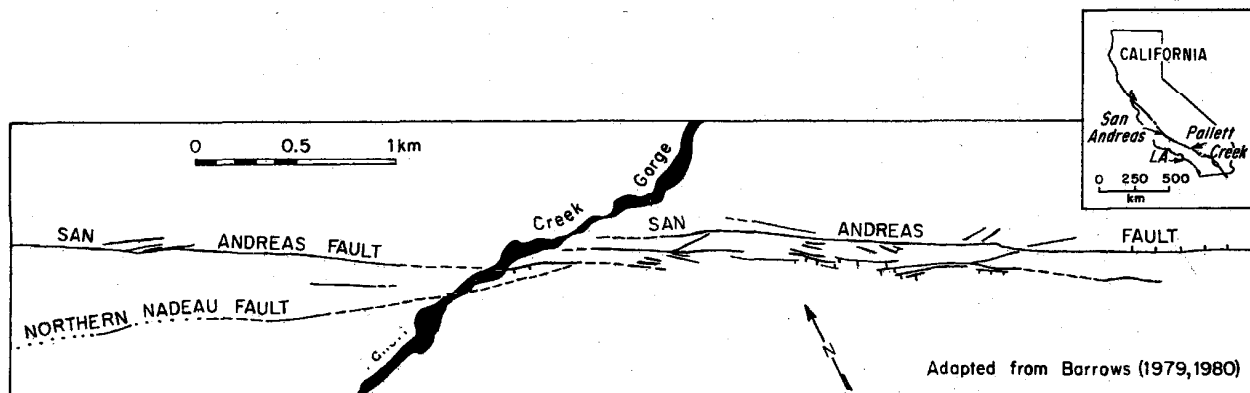


Fig. 1. Geometry of the San Andreas fault in the vicinity of the Pallett Creek paleoseismic site. The fact that the fault steps left in this vicinity lends support to the hypothesis that only a fraction of dextral slip across the fault zone occurs on the discrete faults at the site.

problem. Although the 8-m-thick series of unconsolidated sediments at the Pallett Creek site provides a complete record of the latest 12 large earthquakes [Sieh, 1978a, 1984; Sieh et al., 1989], the rate of right-lateral fault slippage determined is only about 9 mm/yr. This is considerably less than estimates derived elsewhere along the San Andreas fault [Weldon and Sieh, 1985; Schwartz and Weldon, 1987] and far less than values seemingly required by plate tectonic models and geodetic data [Minster and Jordan, 1987; DeMets et al., 1987]. Slip measured for the past three earthquakes, using various piercing points within the excavated sediments, is only 2, 2, and 1.5 m [Sieh, 1984], less than half of the values suggested from offset landforms along the same fault trace several kilometers to the northwest [Sieh, 1978b].

The location of the Pallett Creek site near a major left step in the recent trace of the San Andreas fault (Figure 1) led Sieh [1984] to suspect that significant nonbrittle deformation was present at the site. He speculated that dextral warping and clockwise rotation in the blocks adjacent to the fault would account for the unexpectedly low slip rate determined from the offsets that he measured and dated across faults there. This is not uncommon along strike-slip faults. For example, a fence across the San Andreas fault near Fort Ross, California, also situated near a left stepover in the recent fault trace, experienced a large amount of warping in 1906 (Figure 2), 38% of the total offset that occurred in 1906 occurred as dextral warp in a 130-m-wide zone between the main fault and the extension of the adjacent en echelon fault trace.

STUDY SITE

Three criteria must be met for a paleomagnetic study of crustal rotations to succeed. The unit sampled must have a primary and identifiable magnetization and be isochronous and laterally extensive.

The necessity for a primary magnetization is obvious, as the samples must have recorded and preserved the magnetic field at the time of deposition. Unfortunately, stable magnetization of Holocene sediments adjacent to fault zones is rare. An early attempt at separation of magnetite from one peaty unit at Pallett Creek, unit 61, produced no magnetite (S.-B. R. Chang, personal communication, 1988). In other

samples, secondary magnetic phases and the presence of multidomain magnetite resulted in poor demagnetization behavior and/or inconsistent remanent magnetizations.

The second requirement is that the unit be isochronous. The orientation of Earth's magnetic field changes by as much as 5° in 50 years [Schott, 1896], so sampled horizons must be deposited in far less time than this. If samples from within a unit are not isochronous, differences in magnetization directions may reflect secular variation of the magnetic field, not tectonic rotation.

Finally, to enable sampling across the entire zone of deformation, the unit must be sufficiently extensive and exposed continuously. In addition, samples from areas thought to be beyond the fault zone must be collected to

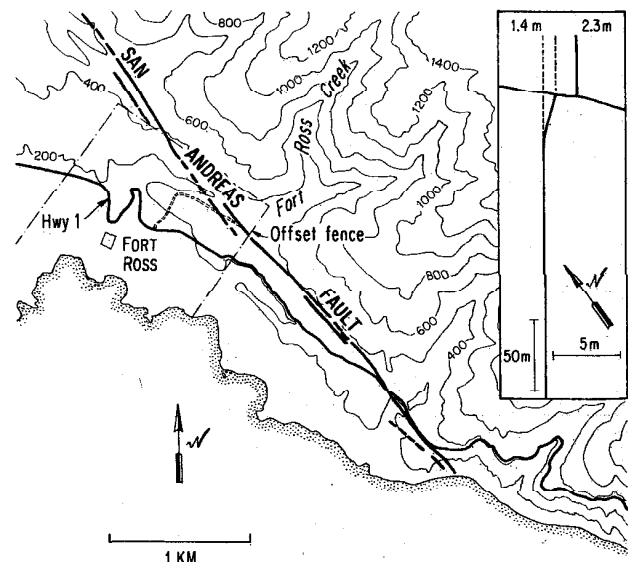


Fig. 2. An example of offset and warping in a setting similar to that at Pallett Creek. This fence line near Fort Ross was offset and warped within the San Andreas fault zone during the 1906 earthquake. Warping occurred in the region of stepover between two fault traces and accounts for 38% of the total dextral offset that was measured. Insert shows the form of the warping with scales showing the horizontal exaggeration [from Lawson, 1908; Brown and Wolfe, 1972; C. Prentice, personal communication, 1988].

provide an initial reference orientation of samples prior to tectonic rotation.

The Pallett Creek paleoseismological site meets all three of these criteria: the sampled beds are isochronous and laterally extensive and have an identifiable primary magnetization. Since about 100 B.C., fluvial and marsh sediments have accumulated rapidly across the San Andreas fault zone at Pallett Creek [Sieh, 1984]. The accumulated sediments alternate between black, organic-rich layers and light to dark brown silts to coarse sands (Figure 3). Excavation of these sediments has revealed 12 individual faulting events in the last 1800 years (Figure 3).

DATA COLLECTION

Our initial analysis of samples showed that units 45, 68, 71, 88, and portions of 61 have stable demagnetization behavior and that units 33, 81, and other portions of unit 61 are unstable. Of the magnetically stable units, units 68 and 71 postdate an incision of Pallett Creek in about A.D. 1100, and so they are laterally extensive. Coincidentally, these units bracket the stratigraphic horizon that was the ground surface at the time of event V, the third earthquake back. Thus the older of the beds, unit 68, has experienced three large earthquakes, and the younger, unit 71, has experienced only two. The top of unit 68 represents the peaty ground surface at the time of event V. Radiocarbon dating shows that this unit was deposited during a period of 60–100 years: its top was deposited within the period A.D. 1479–1503, whereas the base was deposited within the period A.D. 1397–1419 [Sieh *et al.*, 1989].

Unit 71, a 2- to 4-cm-thick, very fine sandy eolian silt [Sieh, 1978a], is present throughout the area and immediately overlies unit 68. Unit 72, a thin peat immediately overlying unit 71, was deposited within the period A.D. 1457–1489. The merged ages of upper unit 68 and unit 72 constrain the age of unit 71, and event V, to A.D. 1480 ± 15 [Sieh *et al.*, 1989], with the expressed uncertainty at the 95% confidence level.

In this study all samples were collected from poorly cemented sediments requiring an appropriate sampling method. We used a sampling tube made of nonmagnetic stainless steel pipe sharpened on one end. The sharpened end was pushed into the trench wall, and its orientation was measured using a Brunton compass. About a quarter of the samples' orientations were also measured with a sun compass, and these declinations generally agreed with the Brunton measurement within $\pm 2^\circ$. The tube was then removed from the trench wall, and we transferred the sample to a quartz glass vial using a plunger. The sediments were cemented in the vial using diluted sodium silicate solution and capped using high-temperature alumina cement.

We collected samples from an excavation cut perpendicularly to the most recent trace of the fault (Figure 4). This excavation extended 50 m northeastward and 3 m southwestward from the fault. Sampling to the northeast was limited by the property line. To the southwest, incision of Pallett Creek early in the twentieth century removed all but the 3 m of the bed nearest the fault.

Figure 4a shows the lateral offsets and vertical deformation associated with the two most recent events. About 2 m of dextral slip occurred across the sampling transect during each of these events [Sieh, 1984]. Figure 4b shows the lateral

offsets and vertical deformation associated with the older, third event. Note that no discrete rupture occurred across the transect, even though as much as 1.5 m of dextral slip occurred only a few tens of meters to the southeast.

Dextral nonbrittle deformation of unit 71 should be added to the 4 m of discrete dextral slip across the fault to derive a more complete measurement of the total dextral slip associated with events X and Z. Dextral deformation of unit 71, subtracted from that of upper unit 68 will give the total value of offset across the transect associated with event V.

Because of its similar tectonic setting, we expected that deformation at Pallett Creek would be similar to the pattern of deformation of the fence line that was deformed during the 1906 San Francisco earthquake near Fort Ross (Figure 2). At Fort Ross, 38% of the total offset occurred as warping in the region between two en echelon fault traces, and the magnitude of the deformation decreased away from the fault trace. The sampling pattern at Pallett Creek was designed to maximize sampling where we expected, from this analogy, to find the largest deformations. From the excavation, we took groups of samples at regular intervals from the fault. The sampling scheme was the same for units 68 and 71. In the meter nearest the fault we took one sample every 10 cm. Between 1 and 20 m from the fault, we collected a group of three samples every meter. We collected a group of three samples every 2 m between 20 and 46 m from the fault. Between 48 and 49 m we collected 10 samples from each unit because we hoped that the magnetization data from this group, collected farthest from the fault, would represent that of undeformed sediments of each unit. The larger number of samples in this control group was intended to provide a mean direction with a smaller uncertainty. Each sample location was surveyed with a three-component electronic surveying instrument (Wild TC2000 "total station") accurate to ± 1 mm in three orthogonal directions.

Progressive demagnetization and measurement of the samples began with alternating field demagnetization in 2.5-mT increments to 10.0 mT. Then, the samples were subjected to progressive thermal demagnetization. About 25% of the samples were demagnetized in 50°C steps to monitor the demagnetization behavior and the remainder were demagnetized in 100°C steps up to at least 600°C. The direction of magnetization components were calculated using a principal component analysis of the demagnetization path [Kirschvink, 1980].

Figure 5 shows typical vector demagnetization diagrams. The samples, in general, showed high stability with one good component of magnetization. We looked for two qualities in determining whether the sample possessed a good quality, or stable, magnetization. The first was less than 10°C, and preferably 5° of variation in the sample direction above 300°C. Although this requirement was usually enough, we also looked for samples with large or erratic variations in magnetic intensity through the demagnetization process. This behavior was usually associated with the large magnetic direction changes. A single sample from unit 71 was removed from our analysis because it had an anomalously high inclination of 83°, although it passed the other two tests. Of the 132 samples of unit 68, 110 showed stable demagnetization, and of the 132 samples from unit 71, 118 were stable.

Because of previous observations that peat layers are magnetically unstable, we chose not to sample peaty uppermost unit 68; instead, we sampled a siltier zone in the center

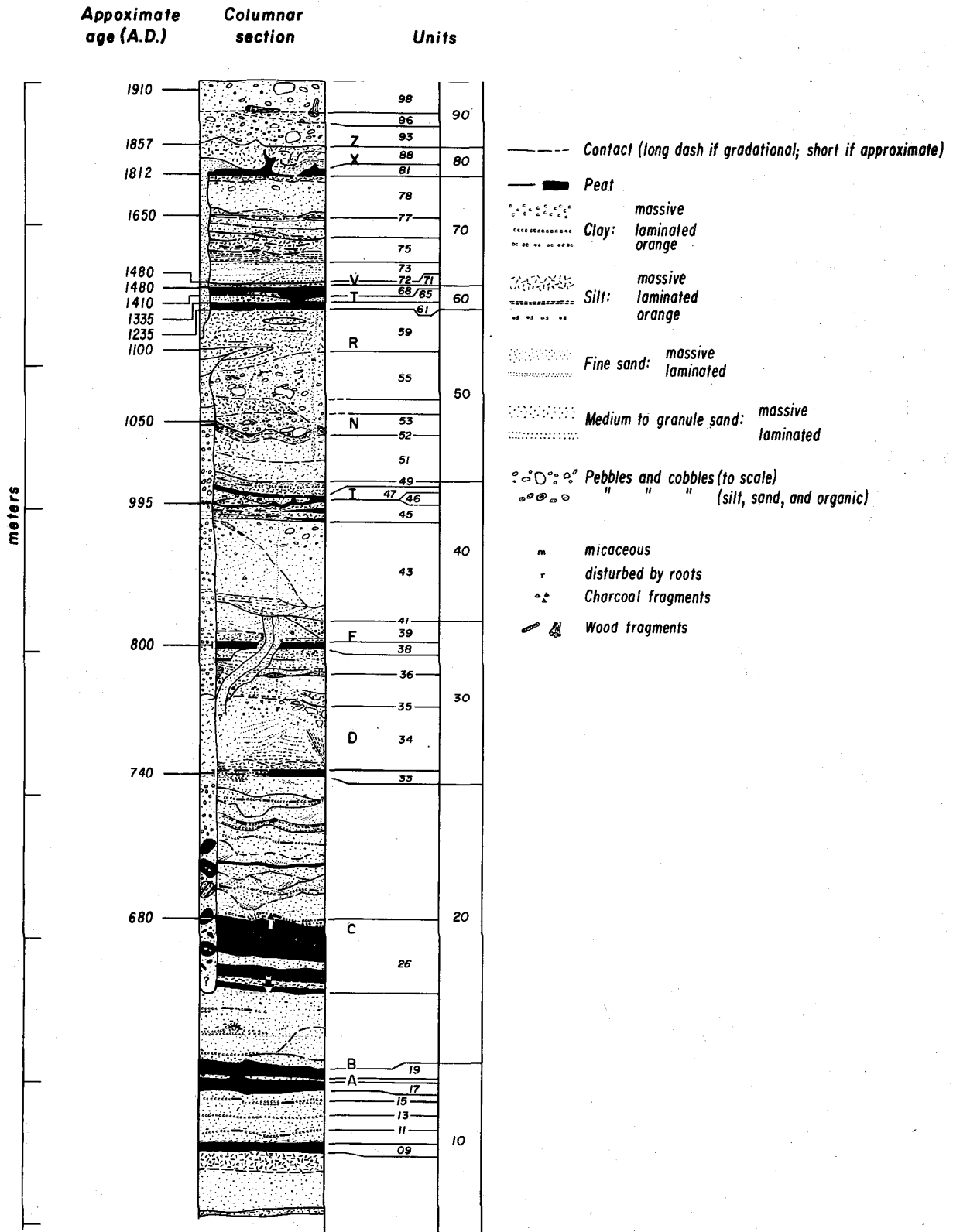


Fig. 3. Late Holocene stratigraphy at Pallett Creek [from Sieh et al., 1989]. Ages of selected units are indicated on the left. The base of the letters on the right corresponds to the ground surfaces at the time of the 12 earthquakes. We analyzed a suite of samples from units 68 and 71, which were deposited just before and just after event V.

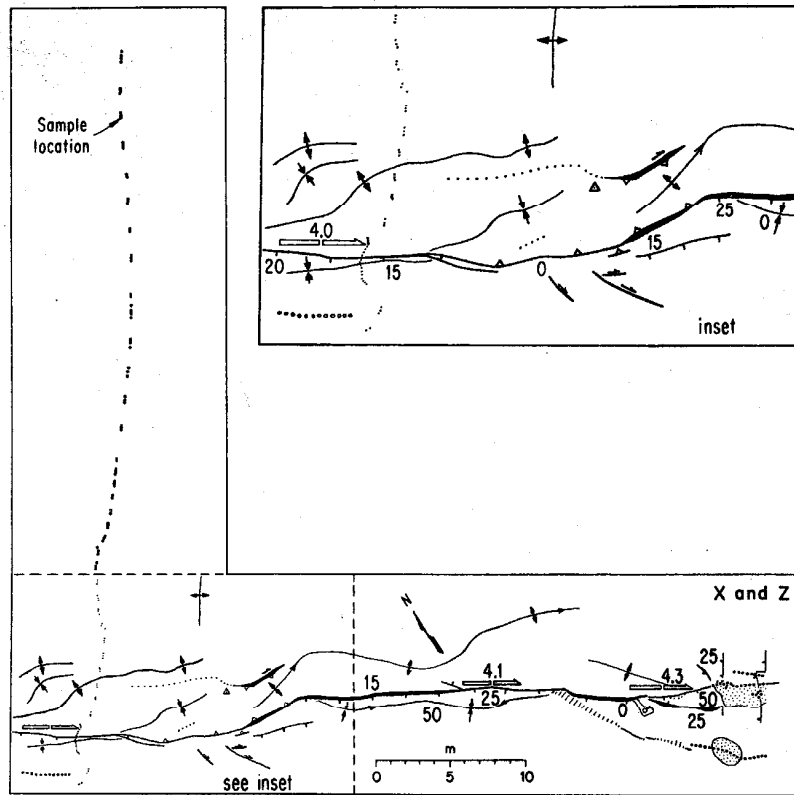


Fig. 4a. Map of sampling traverse for unit 71 and its relationship to traces of faults and folds that were active during events X (A.D. 1812) and Z (A.D. 1857). Open arrows and adjacent numbers indicate dextral slip that occurred during these events. Other numbers indicate vertical offsets (in centimeters). See Sieh [1984] for meaning of other symbols.

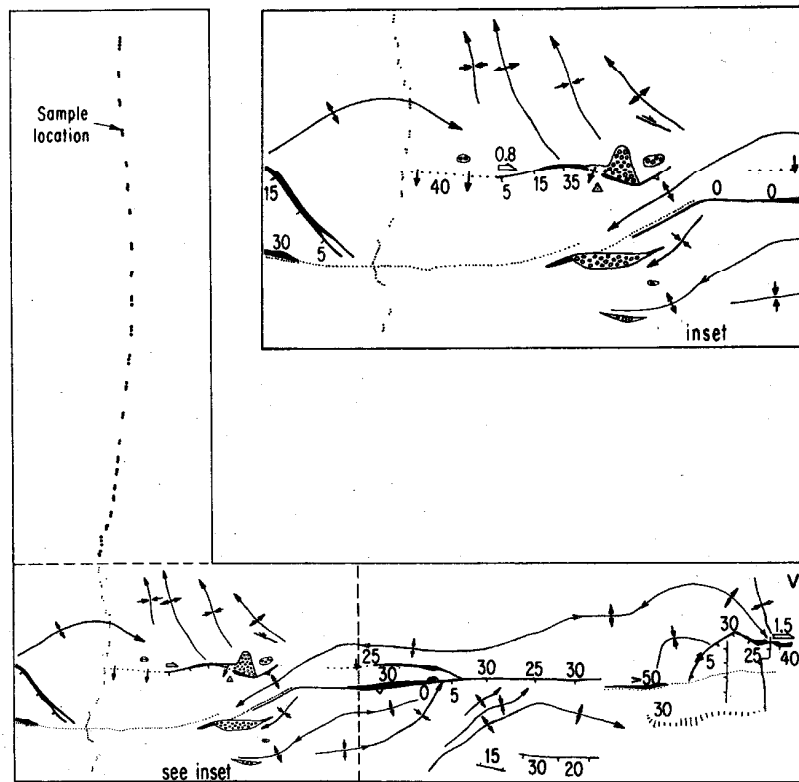


Fig. 4b. Map of sampling traverse for unit 68 and its relationship to traces of faults and folds that were active during event V (about A.D. 1480). See Figure 4a for explanation.

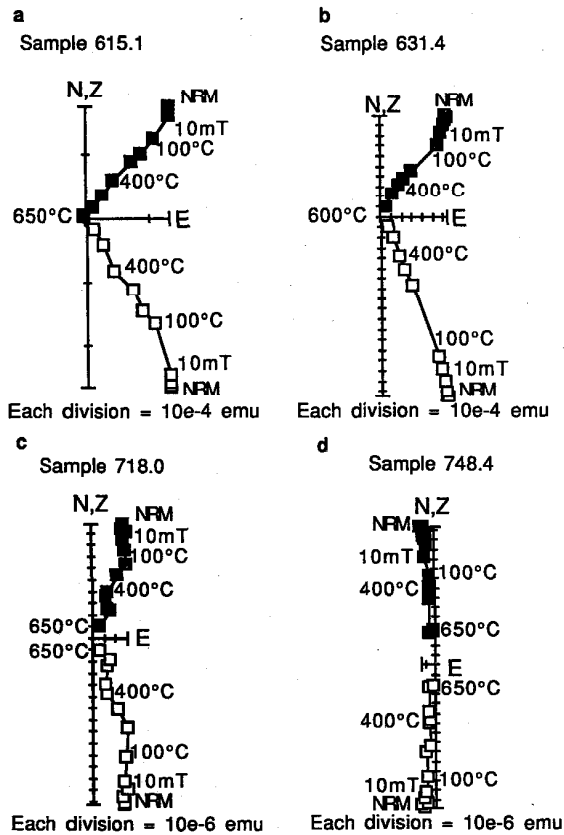


Fig. 5. Orthogonal vector demagnetization diagrams for representative samples. (a) Detrital sample from unit 68. (b) Brush fire sample from unit 68 showing a TRM. (c) Sample from unit 71 and (d) a sample from the unit 71 control group. Solid squares are declination; open squares are inclination.

of the unit. Unfortunately, but unavoidably, this led to poorer control on the age of the sampled stratum, because only the uppermost and lowermost horizons of unit 68 have been dated. These dates bracket the age of the center of the unit between about A.D. 1400 and 1480. In addition, by sampling in the center of the unit there is greater uncertainty in the age equivalency of the samples. The presence of a unique time horizon in unit 68 partially resolves this second concern. In places, the center of unit 68 is a brilliant orange color, suggesting that the normally black peat had been oxidized in a brush fire. Natural remanent magnetization (NRM) intensities of the samples support this hypothesis. These intensities range to values as high as 10^{-2} emu/g, 2–3 orders of magnitude greater than the usual NRM intensities of a good detrital unit. Acquisition of a thermoremanent magnetization (TRM) in a prehistoric brush fire provides the most likely explanation for this orange layer within unit 68. Thus our samples of burned unit 68 acquired their magnetization almost instantaneously, and there is good evidence for a TRM (Figure 5b).

Unfortunately, the peat was not burnt everywhere, and so the orange layer is not ubiquitous. We attempted to maintain synchronicity of the samples, however, by sampling a siltier horizon at locations within unit 68 where the burn layer does not exist. This siltier septum appears to be contemporaneous with the horizon containing the burn.

For each group that consisted of two or three oriented samples, we averaged the sample directions. For unit 68 there were nine groups with three stable samples, 23 groups with two stable samples, and two groups with one stable sample. For unit 71 there were 10 groups with three stable samples, 19 groups with two stable samples, four groups with one stable sample, and one group with no stable samples.

We did not group the samples collected at 10-cm intervals within 1 m of the fault because we wanted to avoid averaging out any rapid changes in amount of rotation at this short distance from the fault.

To eliminate spurious directions due to misoriented or overprinted samples, we employed a simple consistency test. If two of the three samples differed in direction by less than 5° and the third direction was more than 15° away, we considered this third sample an outlier and disregarded it. We admit that this is not a very sophisticated outlier test, but construction of a more sophisticated test for groups of only three samples is not defensible.

RESULTS

The pattern of deformation as recorded in paleomagnetic declinations at Pallett Creek (Table 1 and Figure 6) exhibits these characteristics: (1) Samples nearer the fault generally have more easterly declinations; this suggests greater dextral warping nearer the fault than away from it. However, the scatter in declination values also increases near the fault. (2) Most samples have declinations more eastward than the control groups at 48 m. This indicates clockwise rotation and right-lateral deformation along most of the sample transect. (3) Furthermore, most unit 68 samples show greater clockwise declination than unit 71, an expected result of unit 68 having experienced one more earthquake than unit 71. (4) However, the portion of the transect which contains the groups with the greatest eastward declinations, that is, the section that experienced the greatest clockwise rotation, occurs between 20 and 40 m from the active trace of the fault.

ERROR ANALYSIS

Before the data are discussed in terms of dextral warp, the nature and magnitude of the errors in the data must be investigated. In this study of dextral slip/clockwise rotation, the quantity of greatest interest is the magnetic declination of the sample. Several sources of error are present in these measurements. These sources are (1) collection of samples from different parts of a stratum so that the magnetization in the samples are not isochronous, (2) overprinting of the magnetic direction of the sample, possibly by secondary mineralization or liquefaction, and (3) motion of the sampling tool or misorientation in the field. Because the sampled horizon in unit 68 contains a burn unit and because the units bounding unit 71 have indistinguishable ages, both of these units appear to be isochronous. Therefore the possibility that different parts of the stratum acquired detrital remanent magnetization at significantly different times is remote. However, where the sampling horizon is thinner than the sample size, some of the adjoining material must be sampled. The resulting magnetic direction is an average of all of the directions. However, in all of our samples the accidentally

TABLE 1. Average Group Declinations

Group, m NE of Fault)	Unit 68		Unit 71	
	Number of Samples	Average Declination, °E	Number of Samples	Average Declination, °E
-3	2	0.1	2	0.6
-2	2	2.3	1	6.9
-1	1	13.4	1	-0.8
-0.9	1	-6.8	1	-2.7
-0.8	1	-18.2	1	5.1
-0.7	1	0.3	1	-5.9
-0.6			1	0.8
-0.5			1	-2.2
-0.4	1	0.1		
-0.3	1	37.1	1	12.3
-0.2			1	14.3
-0.1	1	41.5	1	16.5
0.1	1	48.2		
0.2	1	0.4		
0.3			1	2.4
0.4	1	-52.0	1	1.6
0.5			1	-6.0
0.6	1	13.0		
0.7	1	-2.8	1	21.0
0.8	1	-7.0	1	-3.0
0.9	1	40.4	1	-28.7
1	1	-10.4	1	1.6
2	2	31.4	3	5.5
3	2	2.2	2	-1.0
4	3	12.4	3	12.3
5	2	-0.7	2	19.0
6	2	18.8	2	27.8
7	2	-9.6	2	4.3
8	2	-9.9	3	14.1
9	2	9.8	2	1.1
10	2	11.0	2	4.3
11	2	3.9	2	-5.8
12	1	8.0	2	8.1
13	3	-0.3	2	7.4
14	1	16.4	2	2.6
15	3	23.9	2	4.3
16	2	6.8	3	3.7
17	3	20.0	3	-3.1
18	2	20.6	2	-6.6
19	3	23.1	3	8.0
20	2	20.4	3	9.7
22	3	27.4	2	2.6
24	2	15.8	2	9.7
26	2	9.3	2	22.1
28	2	13.4	2	13.9
30	2	36.5	1	12.0
32	2	37.7	1	8.9
34	3	31.4	2	15.4
36	2	-1.2	0	NA
38	2	32.5	1	0.8
40	2	28.6	3	18.6
42	2	13.4	3	12.5
44	3	2.4	2	1.9
46	3	-1.2	3	7.8
48	9	-0.7	6	-1.5

sampled material is only a small fraction of the total volume, and the discrepancy should be minor.

A more serious problem is the possibility of chemical overprinting. The formation of secondary iron oxides after deposition of a unit may complicate the natural remanent magnetization of the sample. If varying amounts formed at different times, the effect is random. This problem is minimized, but not completely eliminated, by the stepwise thermal demagnetization.

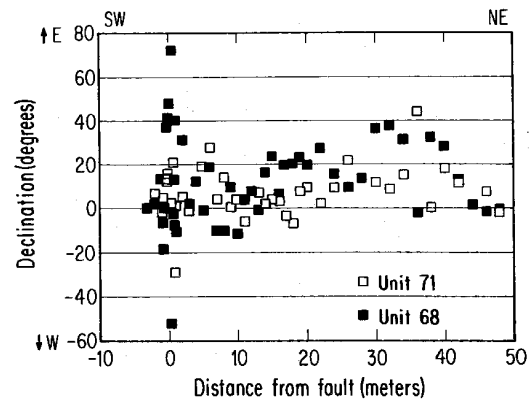


Fig. 6. Group declinations for unit 68 and unit 71. Most sample groups from unit 68, which has experienced deformation during the past three large earthquakes, exhibit larger eastward declinations than overlying sample groups from unit 71, which has undergone deformation during only the past two earthquakes.

A third source of error involves mistakes made during collection and measurement of samples. Samples misoriented during collection probably have the greatest errors, so they are the easiest to recognize and discard. Also, the impact of measurement error is minimized by multiple readings of each component during the measurement process and by conducting a large number of progressive demagnetization steps on each sample.

In spite of these precautions, scatter is still present in the data. Grouping of samples allows application of the consistency test and permits averaging of the data to reduce the random errors. An analysis of the errors is needed to further understand these results.

We begin with the assumption that the data are from a population having a Fisher distribution, which is one of several distributions asymptotically normal on a spherical surface, but circularly symmetric about the mean [Fisher, 1953].

Block Errors

To obtain an initial assessment of the random error in the data, we group the data into blocks of adjacent samples displaying similar declinations. First, we will make the naive assumption that all samples have a uniform rotation and therefore are scattered about the same declination. Table 2 displays the average declination of all of the data between -3 and 46 m. As expected, the scatter is high ($\kappa = 26.9$ for unit 68 and $\kappa = 47.6$ for unit 71). Nevertheless, it is reassuring to note that the average declination of the older unit, 68, is greater than the average declination of unit 71 (12.1° versus 7.1°).

As a refinement of this "block" treatment, we group together the samples from adjacent groups that show similar declinations. Because any rotation should affect unit 68 and unit 71 over blocks of the same dimensions, these groups are the same for each unit. Table 3 lists the results of this grouping. For the most part, this treatment is an improvement over the one-block approximation since the dispersion parameter (κ) is higher for most of the blocks than the values for the large blocks.

This analysis provides one measure of the error in the

TABLE 2. Average Magnetic Orientation of All Samples Between -3 and 46 m

	<i>D</i> , deg	<i>I</i> , deg	<i>N</i>	κ	α_{95}
Unit 68	12.1	41.9	91	26.9	2.9
Unit 71	7.1	40.1	89	47.6	2.2

samples. Because the rotations are of interest and the inclinations are all statistically indistinguishable on these blocks, we continue this analysis using only the declinations. In this case the data are assumed to follow a Von Mises distribution, the circular form of the spherical Fisher distribution [Mardia, 1972].

Group Errors

In this attempt to analyze the errors, we assumed that each sample group was independent and had its own mean and standard deviation. For each group that has two or three samples, we calculate the mean and standard deviation. For the samples within 1 m of the fault we use the sample to either side of a sample to provide a group of two or three samples and then calculate the standard deviation at that location.

Figure 7 shows the data with one-standard-deviation error bars, and Table 4 lists these values. Note that the error bars are quite large. To reduce these uncertainties, we attempt a "group-mean-centered" analysis.

Samples from the same layer, but in different groups, should experience the same effects, except for the magnitude of rotation; thus the groups should be subject to similar random error. Hence it seems reasonable to expect the samples to have a similar amount of angular scatter around the mean direction.

In our group-mean centered analysis, we assume that all of the groups have the same distribution but about different means. Mardia [1972] shows that for circularly distributed data, distributions remain constant through uniform rotation. For the purpose of our error analysis, we rotate each

TABLE 3. Average Orientations of Subsets of the Sampling Traverse

	<i>D</i> , deg	<i>I</i> , deg	<i>N</i>	κ	α_{95}
<i>Unit 68</i>					
-3 to -0.4 m	0.4	38.8	9	28.8	9.7
-0.3 to -0.1 m	38.8	42.2	2	52.1	35.3
0.1 to 3 m	12.9	44.0	13	17.0	10.3
4 to 8 m	10.4	42.8	7	47.7	8.8
9 to 14 m	1.8	38.9	10	35.4	8.2
15 to 19 m	21.0	41.7	13	55.9	5.6
20 to 42 m	21.2	42.2	26	32.0	5.1
44 to 49 m	2.1	40.7	17	66.6	4.4
48 to 49 m	-0.7	40.7	9	142.7	4.3
<i>Unit 71</i>					
-3 to -0.4 m	0.4	39.4	9	23.9	10.7
-0.3 to -0.1 m	14.2	39.1	3	106.6	12.0
0.1 to 3 m	0.4	41.3	12	71.7	5.2
4 to 8 m	15.6	40.0	12	58.2	5.7
9 to 14 m	2.8	37.9	12	93.8	4.5
15 to 19 m	2.0	40.7	13	78.5	4.7
20 to 42 m	12.2	40.9	22	48.0	4.5
44 to 49 m	1.8	38.5	10	132.2	4.2
48 to 49 m	-1.6	37.9	6	95.6	5.6

group so that each has a mean declination of zero. This is akin to a one-dimensional situation where centering the means from two groups with values of 5, 6, and 7 and another with 8, 9, and 10 yields two centered groups of -1, 0, 1. Observation of these centered values shows that the two groups have the same standard deviation. By combining these values into one group, a higher confidence standard deviation for the six measurements can be found.

Using this method, we found that unit 68 has a standard deviation of 4.60° for 82 samples and that unit 71 has a standard deviation of 5.19° for 73 samples. This stacking of the data produces errors much less than those derived from the previous analysis. A more detailed explanation of this analysis is given by Salyards [1989].

Comparison

To test the validity of our assumption that the group-mean-centered standard deviation is a valid representation of the standard deviations of individual sample groups, we compared the standard deviations with an *F* test. This test indicates whether the population group standard deviation is well characterized by the group-mean-centered standard deviation. If the ratio of the variances (standard deviations squared) exceeds the value of the *F* distribution at the 1-0.95 level, the population of standard deviations is judged to be poorly represented by the group mean centered value [Mardia, 1972].

For unit 68 samples the *F* test indicates that 15 of the 33 groups had standard deviations higher than expected, if the group-mean-centered deviations truly represented the whole population. The *F* test indicated, however, that the standard deviations of only six of the 32 unit 71 sample groups were not represented by the group-mean-centered value. These

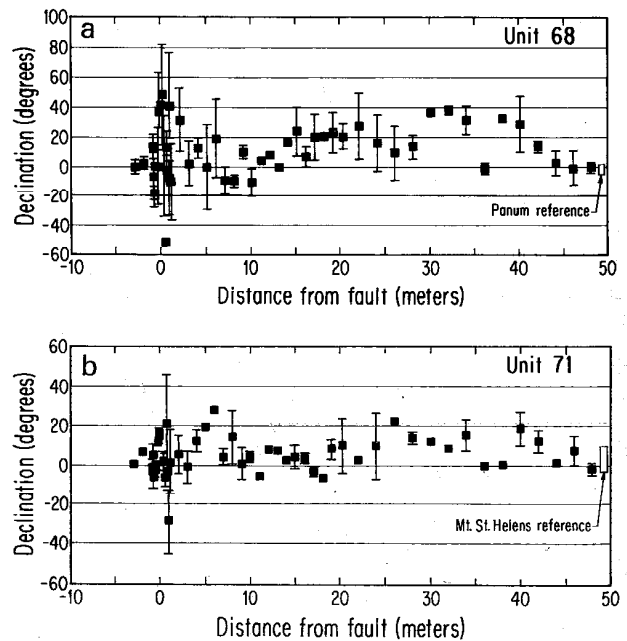


Fig. 7. Group-mean directions with one-standard-deviation errors calculated using the independent group method for (a) unit 68 and (b) unit 71. The open rectangles on the right side of the plots show control directions from Panum Crater (Figure 7a) and Mount St. Helens (Figure 7b).

results suggest that the unit 68 group errors should be treated independently but that the group errors for unit 71 are well represented by the standard deviation of the whole population.

In the ensuing sections we will use the independent group errors in treating unit 68 data, but we will use the group-mean-centered error in our treatment of the unit 71 data.

ABSOLUTE ROTATION

In order to determine the absolute rotation of an individual group we must establish the declination that the group acquired during deposition, prior to tectonic rotation. This declination must be determined independently for both unit 68 and unit 71, because they were deposited a few decades or so apart. The larger sample groups collected 48 m from the fault were taken for this purpose. These samples were deposited far from the mapped fault trace, and so we expected they would have the greatest chance of not being rotated.

The unit 68 sample group from this location has a declination of -0.68° and an inclination of 40.7° . The unit 71 sample group has a declination of -1.6° and an inclination of 38.0° . Three lines of evidence suggest that these directions are unrotated or only minimally rotated.

TABLE 4. One-Standard-Deviation Errors of Group Declinations

Group	Unit 68		Unit 71	
	D, deg	Sigma, deg	D, deg	Sigma, deg
-3	0.1	4.7	0.6	1.4
-2	2.3	4.2	6.9	NA
2	31.4	21.3	55	9.6
3	2.2	14.8	-1.0	8.1
4	12.4	6.6	12.3	5.6
5	-0.7	28.8	19.0	0.7
6	18.8	26.4	27.8	0.7
7	-9.6	9.5	4.3	4.2
8	-9.9	3.8	14.1	13.3
9	9.8	4.4	1.1	8.0
10	-11.0	9.9	4.3	2.6
11	3.9	1.3	-5.8	1.9
12	8.0	NA	8.1	0.1
13	-0.3	1.7	7.4	1.8
14	16.4	NA	2.6	1.9
15	23.9	16.3	4.3	5.9
16	6.8	6.9	3.7	2.5
17	20.0	15.4	-3.1	2.3
18	20.6	2.8	-6.6	0.2
19	23.1	13.5	8.0	4.8
20	20.4	8.3	9.7	13.8
22	27.4	22.3	2.6	1.3
24	15.8	18.9	9.7	16.5
26	9.3	18.2	22.1	0.6
28	13.4	7.8	13.9	2.8
30	36.5	0.8	12.0	NA
32	37.7	2.4	8.9	NA
34	31.4	9.5	15.4	7.8
36	-1.2	3.7	NA	NA
38	32.5	0.5	0.8	NA
40	28.6	18.8	18.6	8.5
42	13.4	3.3	12.5	5.4
44	2.4	8.1	1.9	0.6
46	-1.2	11.6	7.8	7.2
48	-0.7	3.6	-1.5	3.1

NA, not applicable.

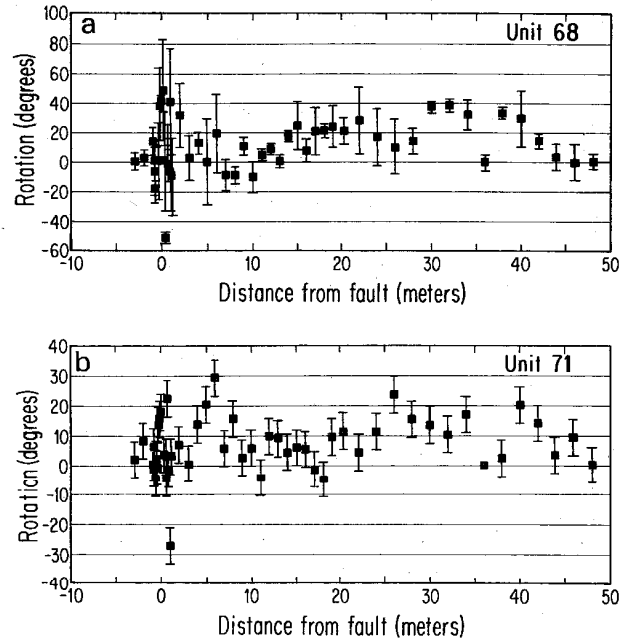


Fig. 8. Group rotations with one-standard-deviation error bars for (a) unit 68 and (b) unit 71.

First, these samples were deposited within meters of the northern wall of the late Holocene gorge [Sieh, 1984]. Although the exact geometry of the gorge wall is unknown, consolidated Tertiary gravel is exposed along the sampling transect 53 m from the fault, that is, only 5 m beyond the control groups. Proximity to this consolidated material might give the samples greater resistance to rotation.

Second, the sample groups nearest the control groups yield the same direction as the control group. This suggests that the material filling the ancient gorge near the gorge wall is not deformed.

Finally, and most importantly, these directions are indistinguishable from unrotated magnetic directions determined from other, tectonically stable sites of the same age. Unit 68 was deposited no more than a century after an eruption of the Mono Craters volcanic chain in about A.D. 1345 (S. L. Salyards and K. E. Sieh, manuscript in preparation, 1992), and unit 71 was deposited within a few years of the A.D. 1482 eruption of Mount St. Helens (R. Hoblitt, personal communication, 1987). To infer the paleomagnetic declinations at Pallett Creek from the declination at these sites, one must make a geographic correction that assumes the earth's field is a dipole. Salyards [1989] determined the errors that result from the fact that the field's nondipole component lends an uncertainty to this correction. His analysis yields an unrotated declination of $-3.2^\circ \pm 3.6^\circ$ for unit 68 (based upon the declination of the samples from Mono Craters) and an unrotated declination of $3.0^\circ \pm 7.7^\circ$ for unit 71 (based upon the declination of samples from Mount St. Helens). The expressed errors are two-sigma values. Both of these directions contain the control group declinations at 48 m, and a similar analysis of the inclinations also contains the control groups.

Using these values and their error bars, Figure 8 and Table 5 show rotations that are the difference in declination between the control group and each sample group. The error

TABLE 5. Angular Rotation and One-Standard-Deviation Errors for Individual Groups

Group	Unit 68		Unit 71	
	D, deg	Sigma, deg	D, deg	Sigma, deg
-3	0.8	5.9	2.1	6.0
-2	3.0	5.6	8.4	6.0
-1	14.1	9.3	0.7	6.0
-0.9	-6.1	16.4	-1.2	6.0
-0.8	-17.5	10.0	6.6	6.0
-0.7	1.0	13.6	-4.4	6.0
-0.6	NA	NA	2.3	6.0
-0.5	NA	NA	-0.7	6.0
-0.4	0.8	26.4	NA	NA
-0.3	37.8	26.4	13.8	6.0
-0.2	NA	NA	15.8	6.0
-0.1	42.2	3.6	18.0	6.0
0	NA	NA	NA	NA
0.1	48.9	34.0	NA	NA
0.2	1.1	34.0	NA	NA
0.3	NA	NA	3.9	6.0
0.4	-51.3	3.6	3.1	6.0
0.5	NA	NA	-4.5	6.0
0.6	13.7	11.7	NA	NA
0.7	-2.1	11.1	22.5	6.0
0.8	-6.3	26.5	-1.5	6.0
0.9	41.1	36.1	-27.2	6.0
1	-9.7	26.1	3.1	6.0
2	32.0	21.6	7.0	6.0
3	2.9	15.3	0.5	6.0
4	13.0	7.5	13.8	6.0
5	0.0	29.1	20.5	6.0
6	19.4	26.6	29.3	6.0
7	-8.9	10.1	5.8	6.0
8	-9.2	5.3	15.6	6.0
9	10.5	5.7	2.5	6.0
10	-10.3	10.5	5.8	6.0
11	4.6	3.8	-4.3	6.0
12	8.7	3.6	9.6	6.0
13	0.3	4.0	8.9	6.0
14	17.1	3.6	4.1	6.0
15	24.6	16.7	5.8	6.0
16	7.4	7.8	5.1	6.0
17	20.6	15.8	-1.6	6.0
18	21.3	4.6	-5.1	6.0
19	23.8	14.0	9.4	6.0
20	21.0	9.0	11.2	6.0
22	28.0	22.6	4.1	6.0
24	16.5	19.2	11.2	6.0
26	10.0	18.5	23.6	6.0
28	14.1	8.6	15.4	6.0
30	37.2	3.7	13.5	6.0
32	38.4	4.3	10.4	6.0
34	32.0	10.2	16.9	6.0
36	-0.5	5.2	NA	NA
38	33.1	3.6	2.3	6.0
40	29.3	19.2	20.1	6.0
42	14.1	4.9	14.0	6.0
44	3.0	8.9	3.4	6.0
46	-0.5	12.2	9.3	6.0
48	0.0	5.1	0.0	6.0

NA, not applicable.

bars represent the square root of the sum of the variances of the reference group and the rotated group.

If the control groups are rotated, the rotations shown in Figure 8 would be shifted upward or downward uniformly. The bars on the right edge of Figure 7 show the range of the Mono Craters and Mount St. Helens declinations and therefore the amount of shift possible.

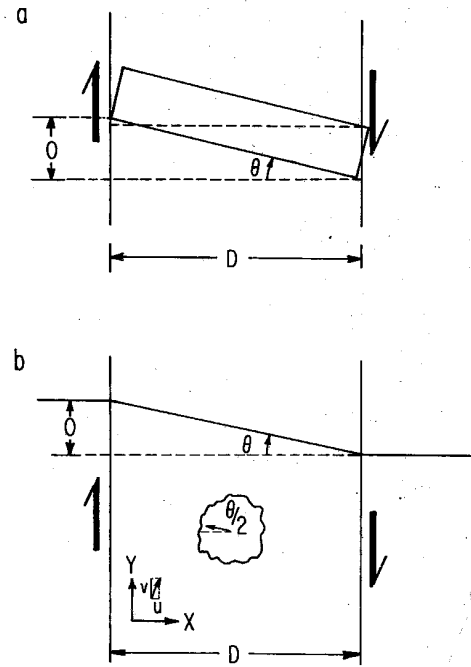


Fig. 9. Conversion of paleomagnetic rotations into strike-slip offset requires the assumption of a deformation model. (a) In the case of block rotation, the offset O equals the tangent of the paleomagnetic rotation angle θ times the length of the block, D . (b) In the case of simple shear continuum deformation, the offset O equals twice the tangent of the rotation angle θ times the length of the block, D .

INTERPRETATION

It is critical to transform the tectonic rotations we have documented into tectonic offset. However, the existence of two possible modes of deformation of the sediments complicates the calculation of the nonbrittle offset based on paleomagnetically inferred rotations. Block rotation is the simpler of these forms of deformation [Nur *et al.*, 1986; McKenzie and Jackson, 1986]. In this case, material rotates as a coherent, rigid block (Figure 9a). The second form of deformation represents a continuum [McKenzie and Jackson, 1983]. In this case the material rotates as small, independent, rigid blocks on the surface of a deforming fluid (Figure 9b). For the case of block rotation, calculation of dextral offset across the block is simple: The offset will be $O = D \tan \theta$, where O is offset, D is distance, and θ is rotation angle (Figure 9a).

In the case of continuum deformation the rotations can be shown to be half of the vorticity of the deforming fluid [McKenzie and Jackson, 1983]. The vorticity is the difference between the y velocity gradient in the x direction and the x velocity gradient in the y direction. Simple shear represents one possible form of this deformation. In this case, deformation in only one direction (in Figure 9b the y direction) means that the velocity in the other direction equals zero. Therefore the vorticity equals the y velocity gradient in the x direction. In simple shear this gradient, and therefore the vorticity, remains constant across the fault zone and its value is O/D . The rotation is half the vorticity, and so solving for the offset, $O = 2D\theta$. This means that the rotation for the simple shear case is approximately half the

rotation in the block rotation case; that is, a simple shear continuum deformation model yields, for a given small rotation, twice the offset of the block rotation model. Obviously, then, our calculation of dextral warping at Pallett Creek is highly dependent on our choice of block rotation or continuum models.

Both of these forms of deformation have been reported in paleomagnetic studies of nonbrittle deformation. *Nelson and Jones* [1987] interpreted the rotations they measured near the Las Vegas Valley shear zone of southern Nevada as being continuum deformation. Based on geologic evidence, Nelson and Jones concluded that the brittle deformation occurred as rotation of small independent blocks, less than 5 km in size, on a deforming, viscous continuum. An example of a study that found rotation of fault bounded blocks is in Dixie Valley, Nevada. *Hudson and Geissman* [1987] found evidence of progressive rotation with less rotation of younger units. However, they also found similar rotation of adjoining ranges suggesting independent blocks rotating together in model like that of *McKenzie and Jackson* [1986].

Block Rotations

We will first calculate the nonbrittle offset across the transect assuming that block rotation has occurred. As we discussed above, the offset across an individual block equals $D \tan \theta$. Figures 10a and 10b show the deformation of unit 68 and unit 71 calculated in this manner. To construct these plots, each segment is centered on a sample group. The ends of each segment are half the distance to the adjacent sample groups. The groups at 48 m from the fault are assumed to be unrotated, so we begin to accumulate deformation at the end of the segment represented by these samples, that is, at 47 m from the fault.

To calculate the error on the sum, we have used the standard deviations shown in Figure 8. However, the standard deviation is in degrees and the quantity being measured is in meters, so a nonlinear conversion is required. We have simply taken the standard deviation of the rotation, added and subtracted it from the rotation angle measured, and calculated the block offset using these angles. To get the errors in meters, we then subtract the mean block offset from the values. Because the summation is a linear combination, the total variance of the sum is the sum of the individual variances.

The dextral warping of unit 68, calculated in this manner, is $14.0 \pm 2.8, -2.1$ m (Figure 10a). Unit 71 shows $8.5 \pm 1.0, -0.9$ m of warping (Figure 10b). The confidence limits shown are one-sigma errors.

Although the calculation of warping as we have implemented it implicitly assumes one sample group per block, this approach does not significantly affect the result. If instead we calculated the offset using our simplistic single block model, the calculated warping would be slightly less at 11.4 m for unit 68 and 7.6 m for unit 71. The multiple block model produces nearly identical results of 14.1 m for unit 68 and 8.7 m for unit 71.

Continuum Deformation

Transformation of the rotations into dextral offset is more complicated in the continuum deformation case as the displacements in both the x and y directions are required. If one

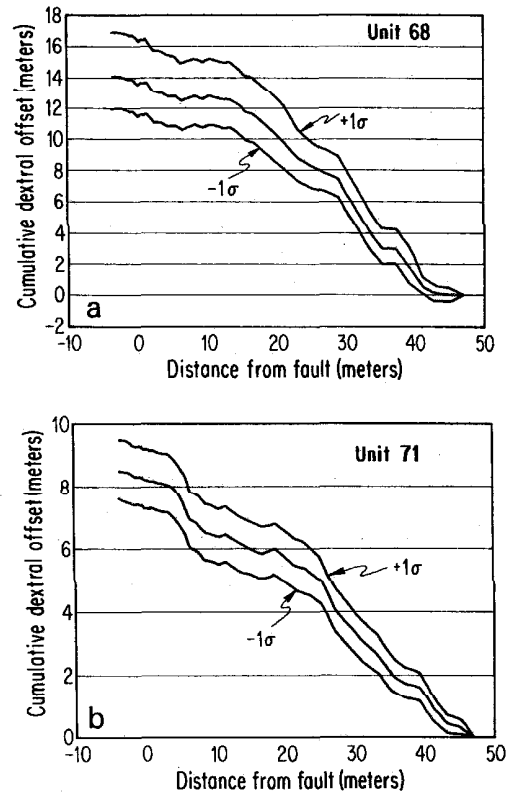


Fig. 10. If one assumes a block rotation model, (a) dextral warping of unit 68 along the sampling traverse is 14.0 ± 2.8 m, and (b) dextral warping of unit 71 is 8.5 ± 1.0 m. A simple shear continuum deformation model yields values twice as large as these. Warping would also be greater if the sampling traverse did not encompass the entire fault zone.

assumes that continuum deformation has occurred as simple shear, one calculates offset of 28.0 m for unit 68 and 17.0 m for unit 71; these offset values are twice those calculated for the case of block rotation.

To find the rotation for a more complicated continuum deformation model, *Salyards* [1989] calculated finite element models of plane strain deformation. In these cases, more complicated fault geometries involving left-stepping fault segments failed to produce rotations exceeding those of the simple shear case. Hence actual offsets in a continuum deformation model must be no more than twice the block rotation values.

DISCUSSION

In a choice between these two models there is only one reason that we favor block rotation rather than continuum deformation of units 68 and 71 at Pallett Creek: the average slip rate determined using the block rotation model is consistent with current kinematic models for the San Andreas fault, whereas continuum deformation models lead to unacceptably high slip rates. If we embrace the block rotation model, the total offset of unit 68 is 18.0 m, 14.0 m of warp and 4.0 m of slip on the fault plane [*Sieh*, 1984]. This represents deformation throughout the last three complete earthquake cycles, that is, between about A.D. 1346 and 1857. The average rate of accumulation of slip between these two dates is thus 35.6 ± 6.7 mm/yr. This rate is indistinguish-

able from the 33.9 ± 2.9 mm/yr late Holocene rate determined for the San Andreas fault at Wallace Creek, about 200 km to the northwest [Sieh and Jahns, 1984]. It is also indistinguishable from the sum of the slip rates across the San Andreas and San Jacinto faults, which merge a few tens of kilometers to the southeast [Weldon and Sieh, 1985; Keller et al., 1982]. If one adopts a continuum model of deformation, slip rates lower than this value cannot be obtained, and rates as high as 62 mm/yr are calculated, if one assumes simple shear. These rates are unreasonable, given that the total relative plate rate between the North American and Pacific plates is 49 ± 3.0 mm/yr [DeMets et al., 1987] and that at least several millimeters of this must be carried by the Elsinore and Newport-Inglewood faults [Millman and Rockwell, 1985; Ziony and Yerkes, 1985].

By adopting the block rotation model we are faced with a significant problem: the lack of cross faulting. In the block rotation model the block in Figure 9a would be bounded on either side with parallel blocks also rotating within the fault zone. Between these blocks would be cross faults accommodating the relative motion of the blocks. The problem is further complicated by our model that divides this large block into at least eight smaller blocks with the implication that some bounding structure should be present between them. With the exception of the main trace of the San Andreas fault and one small splay fault, no bounding structures are observed in the trench exposure.

We argue that our model would make the faults between our subblocks unnecessary, or at the least difficult to observe. Since we have summed the warping across the transect assuming no brittle offset between the blocks, we see no reason why these structures should be observed. Small offsets necessary to accommodate varying amounts of rotation may be taken up over relatively long distances and would be relatively minor in comparison to the site-wide compression [Sieh, 1984].

The cross faults are not as easily dismissed. Since there is no indication of the Pallett Creek site undergoing rotation as a block the size of the site, some form of accommodation zone is necessary.

One possible explanation for the lack of accommodation structures is that we are totally within a rectangular block like that shown in Figure 9a and the sampling did not cross an accommodation structure. The lack of brittle rupture at this point in event V may represent the end of a block, while adjoining blocks had brittle slip and did not rotate as much.

Another possible explanation is that the transect did cross accommodation structures but because they are broader features and insufficient disruption exists to make them observable. Support for this explanation exists in our data. Frequently, a transition region is seen between regions of relatively constant declination (rotation). For example, between 42 and 48 m the rotations drop from 20° to 30° to 0° at the control group. In a similar manner, the accommodation structures may be stretched over 6 m and may be not observable.

Finally, we can not eliminate the possibility that our preferred model is inappropriate. We have simply compared two proven and accepted end-member models. One does not explain the data, while the other does, leaving us to adopt the block rotation model. We welcome future investigations that may validate this model or develop a new family of models that would provide a method of converting paleo-

magnetic rotation into warping and explain the apparent lack of accommodation structures.

It is important to note that in our discussion of the fault behavior, certain aspects are relatively insensitive to the model that we have adopted. Provided that the relationship between paleomagnetic rotation, or the tangent of the rotation angle, and the nonbrittle offset is not too nonlinear, quantities of fault offset can be regarded as relative amounts. A constant scaling factor would convert the block rotation results into offsets for another model. For example, a scaling factor of 2 converts the results into the continuum deformation model.

Our argument in favor of the block rotation model is strengthened by the fact that our sampling traverse may not span the entire fault zone. The traverse is only 55 m long and extends only 3 m southwest of the fault trace. If rotation affected strata farther southwest or northeast, our data would provide only a minimum value for the slip rate.

However, for two reasons, we argue that our 55-m traverse does span the entire zone of deformation. First, slip rates inferred from our data are equal to or significantly greater than the slip rates determined at sites along the fault to the northwest and southeast [Sieh and Jahns, 1984; Weldon and Sieh, 1985]. Second, our sampling traverse spans the en echelon stepover between the two principal faults (Figure 1). Warping should be more severe in this region, because it is in this region that slip is transferred from one fault plane to the other. This is, in fact, seen in the Fort Ross fence (Figure 2). The warping in 1906 occurred only between the en echelon traces, not outside the stepover.

In the discussion of fault behavior that follows, we adopt the values calculated from the block rotation model: 14.0 ± 2.9 m of nonbrittle offset for unit 68 and 8.5 ± 1.0 m for unit 71. When we include the 4.0 m of slip that Sieh [1984] documented across the fault plane, the average slip rate during the three earthquake cycles represented by these strata is 35.6 ± 6.7 mm/yr. Thus we assume that the block rotation model is realistic, and we assume that our sampling traverse encompasses the actively deforming region in its entirety.

These data allow us to evaluate the amount of dextral offset associated with each of the past three large earthquakes at Pallett Creek. Sieh [1978a, 1984] concluded that the amount of slip associated with each event was similar. In the earlier of these papers, he based his conclusion on the fact that vertical deformation associated with each of these events was similar in both style and magnitude. In the later paper, he used three-dimensional excavations to document that the dextral offset across fault planes associated with the A.D. 1480, 1812, and 1857 earthquakes were about 1.5, 2.0, and 2.0 m, respectively. The similarity of these values strengthened his earlier argument that the events were of comparable size. Our data not only strengthen the argument further but also enable a more realistic assessment of the total slip associated with each of these events.

The amount of dextral offset associated with event V (about A.D. 1480) is simply the amount of warping of unit 68 less the amount of warping of unit 71, that is, 5.5 m. Using the error propagation method of summing the variances, that is the square of the standard deviation, of unit 68 and unit 71 (7.8 and 1.0 m², respectively) the one-standard-deviation uncertainty is ± 3.0 m. This 5.5 ± 3.0 m is the total offset, because the sampling traverse fortuitously crosses the fault

zone at a step over in the principal fault planes of event V (Figure 4b). Along this traverse, no brittle faulting occurred during event V.

Dextral offset associated with events X and Z includes both warping and faulting (Figure 4a). We have shown that 8.5 ± 1.0 m of offset occurred as warping. *Sieh* [1984] determined from offset piercing points near our paleomagnetic sampling traverse that a total of 4.0 m of offset occurred across the fault plane during these two events. Thus the combined dextral offset associated with the 1812 and 1857 earthquakes is 12.5 ± 1.0 m.

There is no direct basis for determining how to partition the 8.5 m of warping between the two events. However, for the reasons given below, we estimate that each event produced about half of the warping. First, *Sieh* [1984] showed that each event was associated with 2 m of offset across the fault plane. Second, *Sieh* [1978a] noted that vertical deformation during the 1812 event was nearly identical in style and magnitude to that in the 1857 event. On the basis of these two observations, we divide the 8.5 m of warping equally between the two earthquakes. Hence we estimate that the offset associated with each of these events is 6.3 m, 2.0 m of offset across the fault plane plus 4.3 m of warp.

Given the offset associated with each of the latest three events, we can discuss the most recent history of slip along this segment of the San Andreas fault. Figure 11 shows the history of offsets since about A.D. 1346, assuming, of course, that the block rotation model is valid. Slip magnitudes for each event are based upon data presented in this paper; the earthquake dates are from *Sieh et al.* [1989].

The most remarkable characteristic of this plot is that the offsets do not vary greatly from event to event, despite marked variation in the time between earthquakes. This demonstrates that the segment of the fault represented by the Pallett Creek site does not behave in a time-predictable manner. If earthquakes on this segment of the fault were time-predictable, the length of time between earthquakes would be proportional to the amount of slip during the earthquake at the beginning of the time interval. This relationship is not supported by the data displayed in the figure.

A slip-predictable model can not be completely ruled out. If the earthquakes were slip-predictable, the amount of slip during an event would be proportional to the length of time preceding the event. Because the upper end of the error bar on event X in Figure 11 includes the lower limit of the slip rate, the slip-predictable model possibly describes the behavior of the fault. The amount of overlap is small, and as we discussed earlier, independent evidence suggests a strong similarity between offset in each of the three events. We consider the possibility the fault behaves slip-predictably to be small.

The similarity of slip magnitude from event to event is intriguing. Perhaps the segment of the fault represented by the Pallett Creek site is characterized by a constant strength and always fails when strain equivalent to the observed slip has accumulated. If so, then strain must accumulate quite nonuniformly. During the 134-year-long period between events T and V, it would have accumulated at an average rate of about 41 mm/yr; but between events T and X, it would have accumulated at an average rate of merely 19 mm/yr; and between events X and Z, strain would have accumulated at an astounding rate of about 142 mm/yr!

If one prefers to believe that strain accumulates uniformly

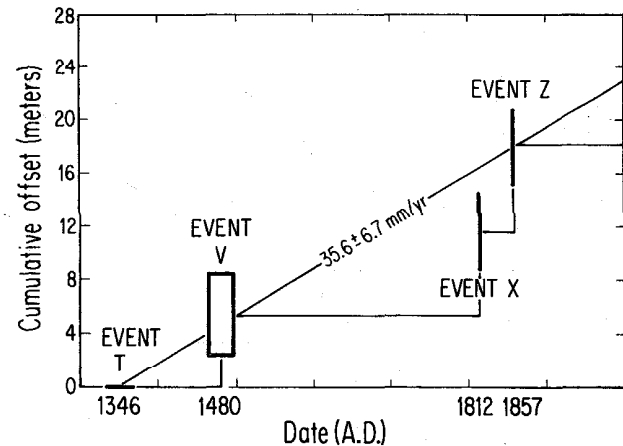


Fig. 11. Slip history of the Pallett Creek site during the past three earthquake cycles. Dates of the past four earthquakes are from *Sieh et al.* [1989]. Slip amounts are based upon fault slip documented by *Sieh* [1984] and warping documented in this paper, assuming block rotation. Errors in earthquake dates are 95% likelihood limits. Errors in dextral offset are one-sigma limits. The slip rate, averaged over the past three earthquake cycles, is about 36 mm/yr; this value is consistent with Holocene rates determined across the fault to the northwest and to the southeast. The amounts of offset during the past three events are similar, about 6 m, even though the interval between events ranges from 44 to about 332 years. These data strongly suggest that (1) the fault has a uniform strength and always sustains 6-m offsets during failure and (2) a time-predictable model is inappropriate for this part of the fault and a slip-predictable model is barely supported.

in the blocks adjacent to the fault, then the data of Figure 11 require one to conclude that fault slip during a large earthquake may not represent complete elastic relief of accumulated strain. To illustrate this, let us compare strain accumulation and strain relief through the three complete earthquake cycles in Figure 11. Between A.D. 1346 and 1480, strain was stored at a rate of 36 mm/yr, so that by the time of event V (1480), 4.8 m of slip would have relieved all the accumulated strain. Within the errors of the data, 5.5 ± 3.0 m occurred in 1480. Following event V, strain built up for a period of more than 300 years. By the time of the next earthquake, 1812, 12 m of slip would have been required to relieve all of the accumulated strain. In fact, only 6.3 m of slip occurred. Thus it appears that only about half of the potential slip occurred. This and a small amount of additional slip that accumulated during the subsequent 44 years were relieved in 1857.

The mechanical reason for such irregular behavior is not immediately apparent to us. Perhaps it is due to a strong interaction between adjacent segments of the fault, as *Rundle* [1988] has suggested, on the basis of his modeling of the behavior of the fault. Or, as *Heaton* [1990] has suggested from his study of the strong ground motions of several modern earthquakes, slip at a particular location along a fault may occur only as a very narrow rupture pulse passes by the site, and, if that pulse passes quickly, not all accumulated strain may be relieved. In this case, the uniformity of slip from event to event would reflect not a constant value of static friction for this segment of the fault but rather constant dynamic parameters such as rupture velocity and length of the rupture pulse. We look forward to the elucidation

tion of the physical explanation for these regular slip events associated with irregular recurrence intervals.

Acknowledgments. We thank Carol Prentice and Charles Budney for assistance in the field and Carol for allowing us to use her mapping near the Fort Ross fence. We also thank R. Hoblitt for allowing us to quote his Mount St. Helens paleomagnetic data. This paper was improved substantially by the thoughtful reviews of J. Geissman, J. Hillhouse, and K. Kodama, and we thank them for their time. This work was supported by U.S. Geological Survey grant 14-08-0001-G1370 and NSF EAR83-51370. Contribution 4135 of the Division of Geological and Planetary Sciences, California Institute of Technology, Pasadena.

REFERENCES

- Barrows, A., Geology and fault activity of the Valermo segment of the San Andreas fault zone, Los Angeles County, California, *Open File Rep. 79-1-LA*, 49 pp., Calif. Div. of Mines and Geol., Sacramento, 1979.
- Barrows, A., Geologic map of the San Andreas fault zone and adjoining terrane, Juniper Hills and vicinity, Los Angeles County, California, *Open File Rep. 80-2-LA*, Calif. Div. of Mines and Geol., Sacramento, 1980.
- Brown, R. D., Jr., and E. W. Wolfe, Map showing recently active breaks along the San Andreas fault between Point Delgada and Bolinas Bay, California, *U.S. Geol. Surv. Misc. Geol. Invest. Map, I-692*, 1972.
- DeMets, C., R. G. Gordon, S. Stein, and D. F. Argus, A revised estimate of Pacific-North America motion and implications for western North America plate boundary zone tectonics, *Geophys. Res. Lett.*, *14*, 911-914, 1987.
- Fisher, R. A., Dispersion on a sphere, *Proc. R. Soc. London, Ser. A*, *217*, 295-305, 1953.
- Heaton, T. H., Evidence for, and implications of, self-healing pulses of slip in earthquake rupture, *Phys. Earth Planet. Inter.*, *64*, 1-20, 1990.
- Hudson, M. R., and J. W. Geissman, Paleomagnetic and structural evidence for middle Tertiary counterclockwise block rotation in the Dixie Valley Region, west-central Nevada, *Geology*, *15*, 638-642, 1987.
- Keller, E. A., M. S. Bonkowski, R. J. Korsch, and R. J. Shlemon, Tectonic geomorphology of the San Andreas fault zone in the southern Indio Hills, Coachella Valley, California, *Geol. Soc. Am. Bull.*, *93*, 46-56, 1982.
- Kirschvink, J. L., The least-squares line and plane and the analysis of paleomagnetic data, *Geophys. J. R. Astron. Soc.*, *62*, 699-718, 1980.
- Lawson, A. C. (Ed.), The California earthquake of April 18, 1906, in *Report of the State*, 2 vol., 641 pp., Earthquake Investigation Commission, Carnegie Institution of Washington, Washington, D. C., 1908.
- Mardia, K. V., *Statistics of Directional Data*, 357 pp., Academic, San Diego, Calif., 1972.
- McKenzie, D., and J. Jackson, The relationship between strain rates, crustal thickening, palaeomagnetism, finite strain and fault movements within a deforming zone, *Earth Planet. Sci. Lett.*, *65*, 182-202, 1983.
- McKenzie, D., and J. Jackson, A block model of distributed deformation by faulting, *J. Geol.*, *143*, 349-353, 1986.
- Millman, D. E., and T. K. Rockwell, Lateral offset of mid- and late-Quaternary deposits along the northern Elsinor fault, southern California, *Geol. Soc. Am. Abstr. Programs*, *17*, 370, 1985.
- Minster, J. B., and T. H. Jordan, Vector constraints on western U.S. deformation from space geodesy, neotectonics, and plate motions, *J. Geophys. Res.*, *92*, 4798-4804, 1987.
- Nelson, M. R., and C. H. Jones, Paleomagnetism and crustal rotations along a shear zone, Las Vegas Range, southern Nevada, *Tectonics*, *6*, 13-34, 1987.
- Nur, A., H. Ron, and O. Scotti, Fault mechanics and the kinematics of block rotations, *Geology*, *14*, 746-749, 1986.
- Ramsay, J. G., and M. I. Huber, *The Techniques of Modern Structural Geology*, vol. 1, *Strain Analysis*, 302 pp., Academic, San Diego, Calif., 1983.
- Rundle, J. B., A physical model for earthquakes, 1, Fluctuations and interactions, *J. Geophys. Res.*, *93*, 6237-6254, 1988.
- Salyards, S. L., Dating and characterizing late Holocene earthquakes using paleomagnetism, Ph.D. thesis, 225 pp., Calif. Inst. of Technol., Pasadena, 1989.
- Schott, C. A., Secular variation of the earth's magnetic force in the United States and in some adjacent foreign countries, annual report, Appendix 1. U.S. Coast and Geod. Surv., Washington, D. C., 1896.
- Schwartz, D. P., and R. J. Weldon, San Andreas slip rates: Preliminary results from the 96 St. site near Littlerock, CA., *Geol. Soc. Am. Abstr. Programs*, *19*, 448, 1987.
- Sieh, K. E., Prehistoric large earthquakes produced by slip on the San Andreas fault at Pallett Creek, California, *J. Geophys. Res.*, *83*, 3907-3939, 1978a.
- Sieh, K. E., Slip along the San Andreas fault associated with the great 1857 earthquake, *Bull. Seismol. Soc. Am.*, *68*, 1421-1428, 1978b.
- Sieh, K. E., Lateral offsets and revised dates of large prehistoric earthquakes at Pallett Creek, southern California, *J. Geophys. Res.*, *89*, 7641-7670, 1984.
- Sieh, K. E., and R. H. Jahns, Holocene activity of the San Andreas fault at Wallace Creek, California, *Geol. Soc. Am. Bull.*, *95*, 883-896, 1984.
- Sieh, K. E., M. Stuiver, and D. Brillinger, A more precise chronology of earthquakes produced by the San Andreas fault in southern California, *J. Geophys. Res.*, *94*, 603-624, 1989.
- Thatcher, W., and M. Lisowski, Long-term seismic potential of the San Andreas fault southeast of San Francisco, California, *J. Geophys. Res.*, *92*, 4771-4784, 1987.
- Weldon, R. J., II, and K. E. Sieh, Holocene rate of slip and tentative recurrence interval for large earthquakes in the San Andreas fault, Cajon Pass, southern California, *Geol. Soc. Am. Bull.*, *96*, 793-812, 1985.
- Ziony, J. I., and R. F. Yerkes, Evaluating earthquake and surface-faulting potential, in *Evaluating Earthquake Hazards in the Los Angeles Region*, edited by J. I. Ziony, *U.S. Geol. Surv. Prof. Pap.*, *1360*, 43-91, 1985.

J. L. Kirschvink and K. E. Sieh, Division of Geological and Planetary Sciences, California Institute of Technology, Pasadena, CA 91125.

S. L. Salyards, Geophysics Program, New Mexico State University, Las Cruces, NM 88003.

(Received March 19, 1990;
revised October 10, 1991;
accepted January 27, 1992.)